Oil ganglia dynamics in natural porous media during surfactant flooding captured by ultra-fast x-ray microtomography

Souhail Youssef[1], Elisabeth Rosenberg[1], Herve Deschamps[1], Rezki Oughanem[1-2], Eric Maire[2], Rajmund Mokso[3]
[1]IFP Energie nouvelles, [2] INSA-Lyon MATEIS CNRS UMR 5510, [3] Swiss Light Source, Paul Scherrer Institut,

This paper was prepared for presentation at the International Symposium of the Society of Core Analysts held in Avignon, France, 11-18 September, 2014.

ABSTRACT

We have conducted a set of experiments (drainage, imbibition and surfactant injection) at the TOMCAT beam line of the Swiss Light Source (SLS) on sandstone samples. 3D images of oil ganglia trapping during the imbibition sequence and their mobilization during the surfactant injection sequence have been captured at different capillary numbers. 3D Images were taken with a voxel size of 5 µm and a time interval of 3 s and then reconstructed using a phase contrast algorithm. Results show that at intermediate capillary numbers and relatively high residual oil saturation oil ganglia tend to coalesce and form a large cluster before being evacuated. This mechanism is likely to be at the origin of oil bank formation. At high capillary number and low residual saturation, ganglia are eroded and pulled off before being removed individually. After image processing, we have extracted different global and local descriptors like the mean residual saturation, saturation profiles, size distribution of oil ganglia and the largest cluster size for each time step. We have found that the mean ganglia size decreases as a function of the capillary number whereas the largest cluster increases immediately after increasing the capillary number and then decreases.

INTRODUCTION

Enhanced Oil Recovery using surfactant is a process of great interest for oil production because it can potentially decrease the capillary trapped oil by a large amount. The principal difficulty in oil mobilization lies in the fact, that non-wetting fluids are trapped as disconnected components (clusters and ganglia) under important capillary forces [1]. These forces are strongly related to the geometry of the pore network, the fluid-fluid properties (interfacial tension) and the fluid-rock properties (wettability) [2]. We can distinguish two main local trapping mechanisms that occur during waterflooding of water wet rock: the snap-off induced by the collapse of the wetting phase in the pore throat and the by-pass cutoff described by the pore doublet model [3, 4].

In natural porous media, these mechanisms have been observed only recently [5, 6]. Once oil is trapped the objective of surfactant injection is to create flow conditions, during which displacing forces (viscous or gravity) dominate capillary forces [7]. Indeed

surfactant injection induces a better microscopic displacement efficiency by reducing the interfacial tension between trapped oil and water and facilitates the formation of an oil bank. During surfactant flooding and more generally during high capillary number flooding several complex physical phenomena including oil ganglion mobilization, breakup, stranding and coalescence can take place. These mechanisms have been predicted theoretically in [8] and observed experimentally in 2D and 3D transparent micromodel in [9-11]. Trend and correlation of oil ganglia size as a function of capillary number have also been proposed in [12-14]. These studies show that the maximum ganglion size decrease while increasing the capillary number and that the mean ganglion size is a power law of the capillary number.

Imaging ganglion dynamics in natural porous media was not possible until recent developments in synchrotron based x-ray tomography [15]. Due to both the high photon flux of synchrotron radiation and a high speed camera, fluid flow in natural porous media can be imaged with few seconds to sub-second temporal resolution and a spatial resolution ranging from 2 to 20 μm [5, 6]. Experiments are conducted in a miniaturized flow cell specifically developed to perform in-situ computed microtomography (μCT) multiphase flow and allowing a precise control of the experimental conditions (flow rate, pressure and temperature) [16].

In this paper we first present the experimental set up that allows in situ dynamic acquisition of 3D images with a spatial resolution of 5μm and a time interval of 3s. Then we discuss the results at the core scale and pore scale of three cycles of injection (drainage, spontaneous imbibition and surfactant flooding) in a water wet sandstone. Finally we describe the behavior of oil ganglion during surfactant injection.

METHODS AND MATERIALS

Imaging setup

The experiments were carried out at the TOMCAT beamline [17] at the Swiss Light Source. The sample was exposed to a parallel filtered polychromatic x-ray beam (pink beam) with a peak energy at around 25 keV. The transmitted x-ray was converted into visible light by a 100 μm LuAG scintillator and projected onto a high speed CMOS camera. The camera (pco.Dimax) is a 12-bit camera with 2016x2016 pixels and a physical pixel size of 11x11 μm². The image formed by the scintillator was projected at the detector sensor with a 2.2x magnification resulting in an image pixel size of 5 μm. As the onboard memory of the camera is limited to 36 GB, the number and size of the acquired images have to be optimized to satisfy different parameters (image quality, time interval, total acquisition time) before pausing for image transfer. The acquisition parameters were set as follow. The field of view was restricted to 1008x1008 pixels. The number of projections for one tomogram was set to 500 over 180°, with an exposure time of 2 ms per projection. A pause time of 2 s was fixed between each set of 500 projections. The chosen configuration allows for the acquisition of 50 tomograms, with an acquisition time of 1 s per 3D image and a total acquisition time of 150 s.

Flooding experiments

The dry sample is mounted in a PEEK Hassler type core holder especially designed to allow 3D image acquisition with a pixel size of 5 μm and an in-situ monitoring of the fluid saturations during the experiment. The core holder is fixed on the rotation stage with a sample-to-detector distance of 300 mm (the setup is illustrated in Figure 1). Each side of the core holder is equipped with three ports (inlet, outlet and pressure tap). The top inlet is connected to the oil pump and the bottom inlet is connected to the brine and the surfactant pumps. All the fluids are injected by HPLC type pump located outside of the experimental hutch at approximately 10 m from the core holder. The outlet ports are connected to a digital pressure controller to monitor the pore pressure. The pressure taps are connected to a differential pressure transducer. Two additional ports are used to control the confining pressure. All ports are connected to flexible tubing that allow the core holder to rotate over 240° without inducing any tangential stress.

To achieve the dynamic image capture, the core holder is allowed to rotate during 1 s over 180° at a constant speed calculated from the frame rate of the detector. The 2 s time interval between two images is used for initializing the core holder position to its initial angular position. This cycle is then repeated fifty times before stopping the acquisition to free the camera memory and transfer the projections to the reconstruction server. During the transfer time that lasts 30 min, the sample is maintained under steady state condition.

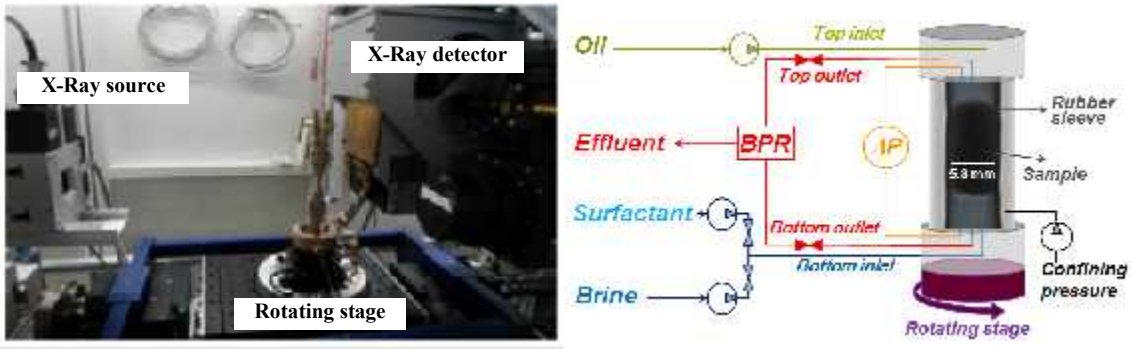

Figure 1. Setup for the dynamic flow imaging experiment with (a) TOMCAT beamline endstation and (b) schematic representation of the core holder modules connection.

Three acquisition cycles are conducted during the flooding experiments corresponding to a drainage phase, spontaneous imbibition with brine and surfactant injection at different flow rate. The experiment begins with the sample 100% saturated with brine. The confining pressure and pore pressure are respectively set to 8 bar and 4bar. The first set of images is acquired while the oil is injected from the top at two successive flow rate (0.5 and 1 cc/min). The top outlet of the cell was closed and the bottom face was swept with brine at a rate of 0.06 cc/min. In the second cycle, oil injection is first stopped while the bottom face remains swept with brine allowing the sample to undergo a counter-current imbibition. Then the top outlet is opened to generate a co-current imbibition. During the third cycle of acquisition a surfactant solution is injected from the bottom at five different flow rates (0.05, 0.2, 0.5, 1.4 and 4 cc/min). The flow rate is increased every 30 s.

Image reconstruction and processing

In the aforementioned experimental setup sample-to-detector distance was set to 300 mm to generate an optimal propagation-based phase contrast [18]. The tomographic reconstruction is made in two steps. First a phase retrieval algorithm is applied to all projections to extract phase and intensity maps [19]. Then the *gridrec* algorithm [20] is used for 3D image reconstruction. Figure 2 shows a slice of the studied sample at an intermediate oil saturation. We can clearly distinguish the different phases present in the sample (oil, brine and minerals). This is confirmed by the gray level histogram that exhibits three different peaks corresponding to the oil phase, brine phase and mineral matrix. The good quality of images is essential to develop a fully automated image processing workflow.

The three cycles of acquisition generate a 4D dataset of 150 tomograms with a total size of 310 GB. To process this time series of 3D images, we have developed a reproducible and reliable automatic quantitative analyze procedure based on the open-source ImageJ project. First images are registered and cropped in a cylinder of 800 voxel in diameter and 800 voxel in length (corresponding to a diameter of 4 mm and a length of 4 mm). Then the gray level is rescaled and converted in 8 bits. At this stage gray level histograms and mean gray profiles are extracted. Afterwards the images are segmented using histogram methods [21]. Figure 2 shows the results of the segmentation where we can see that the different phases and interfaces are well defined. Finally the connected components of the oil phases are labeled and the corresponding volumes are extracted. Volume visualization and rendering can then be performed with Avizo.

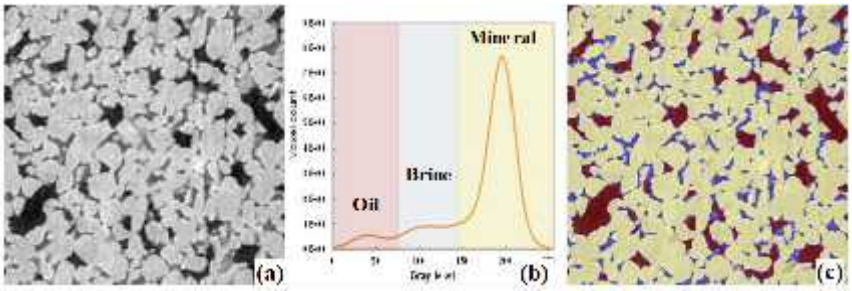

Figure 2 (a) A tomographic slice of Bentheimer sandstone at intermediate saturation reconstructed using phase retrieval method and the corresponding (b) gray level histogram. (c) Resulting segmented image.

Sample and fluids

The studied sample was cored in a strongly water-wet Bentheimer sandstone with 22% mean porosity and a permeability of 3.8 D. The dimension of the miniplug was 5.8 mm in diameter and 8 mm in length. The displacement experiments were conducted using potassium iodide brine (40 g/l KI) and n-Decane. The surfactant solution was prepared by adding 0.025 wt. % of dodecyl benzene sulfate (SDBS) and 5 % of isobutyl alcohol to the brine phase. The brine, the surfactant solution and the n-Decane viscosity are respectively 0.93, 1.11 and 0.93 cP at 22 °C. The interfacial tension between n-Decane and surfactant solution, measured by spinning drop method, is 0.3 mN/m.

RESULTS AND DISCUSSION

Preliminary observations

Figure 3 shows a tomographic time-series slices of a small field of view (few pores) depicting the full sequence of flooding: drainage, spontaneous imbibition and surfactant injection. During the drainage (slices 1 to 3) the largest apparent pores are invaded by oil quasi instantaneously (we did not capture an advancing meniscus even with a time interval of 3 s). However during the spontaneous imbibition (slices 4 and 5) only the smallest pores and throats are invaded with brine. After the spontaneous imbibition the oil remains trapped in the largest pores. To mobilize the trapped clusters, viscous forces must overcome the capillary forces at the origin of the ganglia blocking phenomena. In other words the capillary number (Nc) which represent the ratio of those two forces must be increased. At the laboratory scale Nc can be increased either by increasing the flow rate and the viscosity of the wetting phase or by lowering the interfacial tension (IFT) between oil and brine. In our experiment we have first decreased the IFT at an intermediate value (0.3 mN/m) and then progressively increased the flow rate of the surfactant solution to cover an Nc range between 10^{-4} and 10^{-2}.

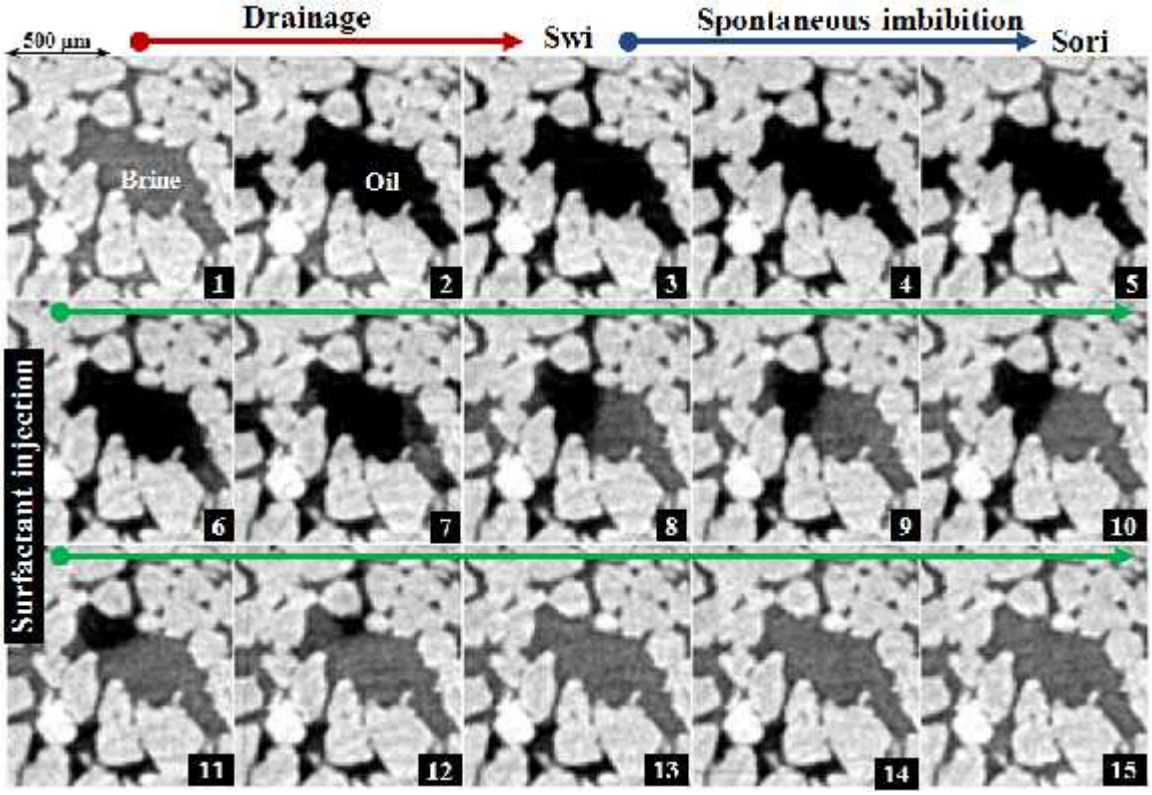

Figure 3 Tomographic time-series slices captured during drainage (1to3), spontaneous imbibition (4 and 5) and surfactant injection (6 to 7) in the Bentheimer sandstone. Oil is black, brine intermediate gray and mineral light gray.

During the surfactant injection (slices 6 to 15) we can clearly see the progression of an oil/brine interface within the largest pore. The oil ganglion is evacuated progressively through the largest throat. Those first observations on 2D slices already show the complexity of pore scale dynamic behavior of two phase flow.

Once images are processed and segmented 3D image visualization allows to investigate the dynamic progression of the fluid invasion. As it is not possible to show all the images, we have selected in Figure 4 a set of images representing different steps during the flooding cycle: end of drainage (Swi), end of spontaneous imbibition (Sori) and four images captured during surfactant injection corresponding to the end stage of four flow rates. At Swi (first image) we see that oil occupies a large part of the pore space as one single percolating cluster. At Sori (Figure 4 (1)) the oil saturation has decreased. At this step the oil phase is not any more percolating. Indeed the oil phase is trapped as isolated cluster and ganglia. As soon as surfactant reaches the sample, the oil phase begins to move. At the lower flow rate (0.05 cc/min) few visual changes are observed which are mainly interfaces rearrangement (this point will be discussed later). By increasing the flow rate more and more oil moves toward the top of the sample. Large changes are observed at each rate change as well as an acceleration of the oil flow rate. At the end of the fourth stage which correspond to a flow rate of 1.4 cc/min almost all the oil has been evacuated.

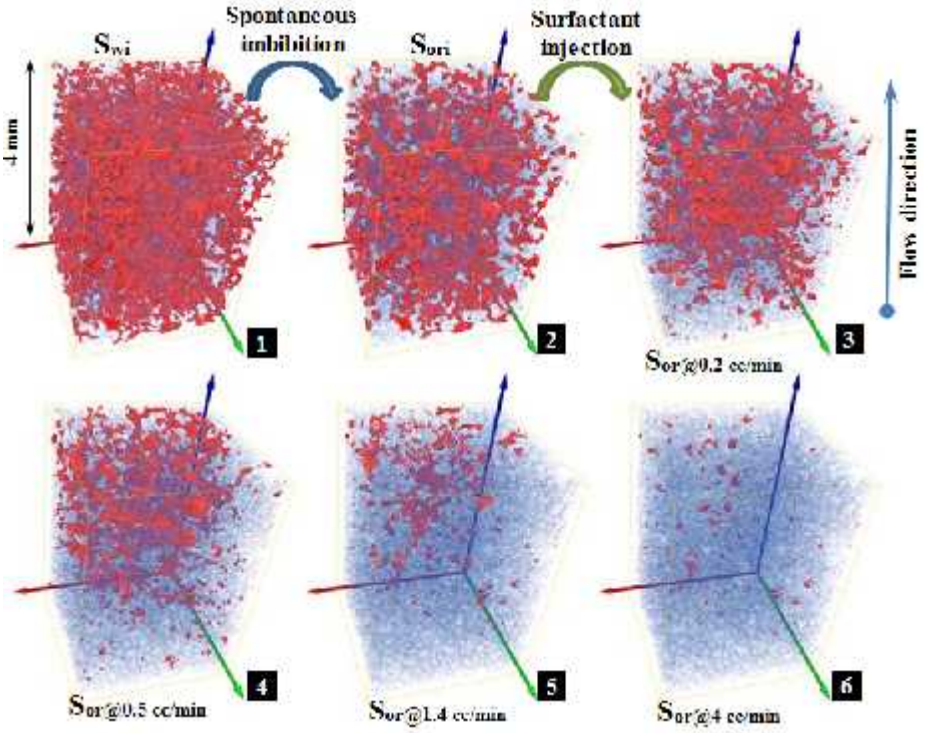

Figure 4 3D images sequence of the imbibition and surfactant injection process in a the Bentheimer sandstone. The mineral phase is removed, the brine is transparent blue and the oil phase in red. Image1 represents the 3D oil phase distribution at Swi, image 2 at Sori and images 3 to 6 at intermediate steps during surfactant injection.

Core scale quantitative analyses

To get more insight into the oil saturation evolution during the different flooding steps, mean oil saturation is computed for each image of the time series. Figure 5 represents the oil saturation as a function of time. The three cycles are represented in different colors (drainage in red, spontaneous imbibition in blue and surfactant flooding in green). During the drainage cycle we observe two saturation bumps corresponding to the two successive flow rates. The time interval allows to capture the transient part of the oil invasion. We can see that the increase in oil saturation rate is more important at the beginning of each bump. Observation of the dynamic 3D images shows that multiple pores are invaded simultaneously during one acquisition time interval. For example between the images at 75 s and at 78 s almost 2000 pores have been invaded which corresponding to an increase in the oil saturation of 10%. This avalanche behavior happened because first the pore size distribution is quite narrow and then the imposed flow rate generates immediately a sufficiently high pressure in the oil phase to overcome the capillary forces imposed by the pore necks. At the end of the drainage we reach 52 % of oil saturation.

During the imbibition cycle we also observe two stages of saturation. The first stage is generate by the counter current spontaneous imbibition. We observe a moderate decrease in the oil saturation (4%) during 6 s. 3D images show that during this step few small pores are invaded by brine but the main changes take place at the interfaces. We observe a relaxation of the interfaces corresponding to a decrease in its curvature. The second decrease in the saturation is provoked by the co-current imbibition. This imbibition step is also very fast and occurs in less than 9 s resulting in an expulsion of 13% of oil and the disconnection of the oil phase. The residual oil saturation (S_{ori}) remains constant during the rest of the imbibition cycle at a value of 35%

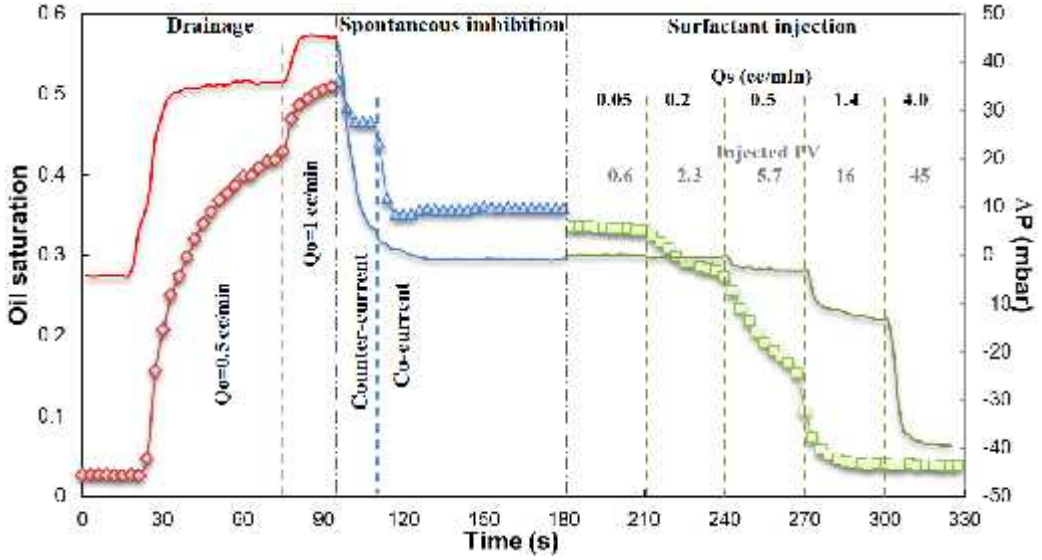

Figure 5 Time evolution of oil saturation in the Bentheimer sandstone (points) and the corresponding pressure drop (continuous line). The red points correspond to the drainage cycle at a rate of 0.5 cc/min and 1 cc/min, the blue points to the spontaneous imbibition cycle and the green points to the surfactant injection cycle at five successive flow rates: 0.05, 0.2, 0.5, 1.4, and 4 cc/min (total pore volume (PV) for each flow rate are : 0.6, 2.3, 5.7, 16, 45)

Image acquisition of the surfactant injection cycle begins at a saturation of 32% (green points). This first decrease in the oil saturation compared to S_{ori} shows that the surfactant solution has already reached the sample. During this cycle, the oil saturation curve shows three inflection points corresponding each time to an increase in the flow rate. As observed on 3D images the rate of oil evacuation is also increased with increasing the flow rate. At the end of the first and second stage the saturation seems to stabilize while in the third stage we did not reach a steady state before changing the flow rate. At the end of the fourth stage which corresponds to a flow rate of 1.4 cc/min the remaining oil saturation is 4%. Increasing the flow rate to 4 cc/min didn't produce more oil. Figure 6 shows the water saturation profiles acquired during the surfactant injection cycle. These profiles show that the injection of the surfactant solution generates a gradient of saturation along the sample. Profiles corresponding to the two first stages show that the oil has been removed only from the first half of the sample. The second part of the sample begins to desaturate at the third flow rate injection stage. This observation suggests that the viscous forces needed to mobilize trapped oil are not reached all along the sample.

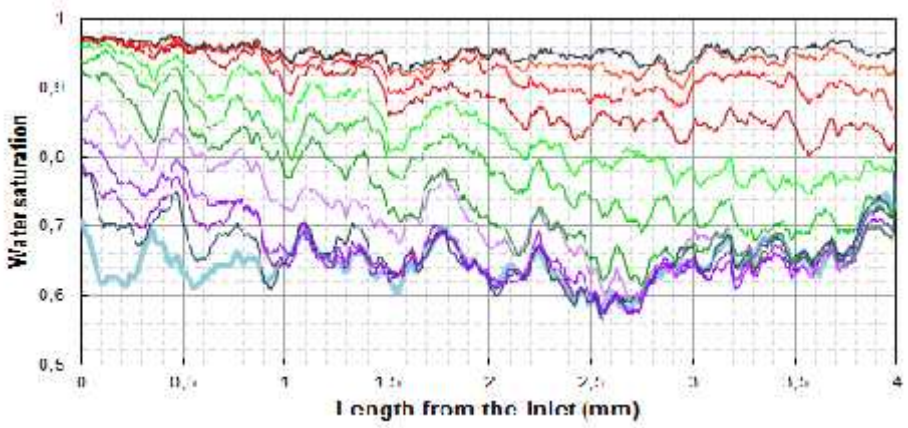

Figure 6 Saturation profiles along the Bentheimer sandstone sample during the surfactant injection cycle. The injection is done from the 0 abscisse side. The different groups of colour (blue, purple, green, red and black) correspond respectively to the five flow rates (0.05, 0.2, 0.5, 1.4 and 4 cc/min).

Pore scale analyses

In this section we will focus on the local mechanisms that govern the trapping of oil ganglion during the spontaneous imbibition and then we present some aspects of ganglion dynamics during surfactant flooding. Figure 7 shows 3D images time series zoomed at the pore scale during the spontaneous imbibition cycle. During the counter-current stage (image 1 and 2) we observe mainly meniscus receding. This phenomena leads to an increase in the interface curvature and consequently a decrease in the local capillary pressure. As soon as the co-current imbibition begins (image 3 and 4) snap-off take place and the largest pores are bypassed through the smallest ones leading to the trapping of an oil ganglia. The statistic analysis shows that the mean radius of the pore invaded by brine is 36.5 µm while the mean radius of the pore containing oil is 62.2 µm. This confirms the fact that oil is trapped in the largest pore (mean pore radius in the sample is 52.2 µm).

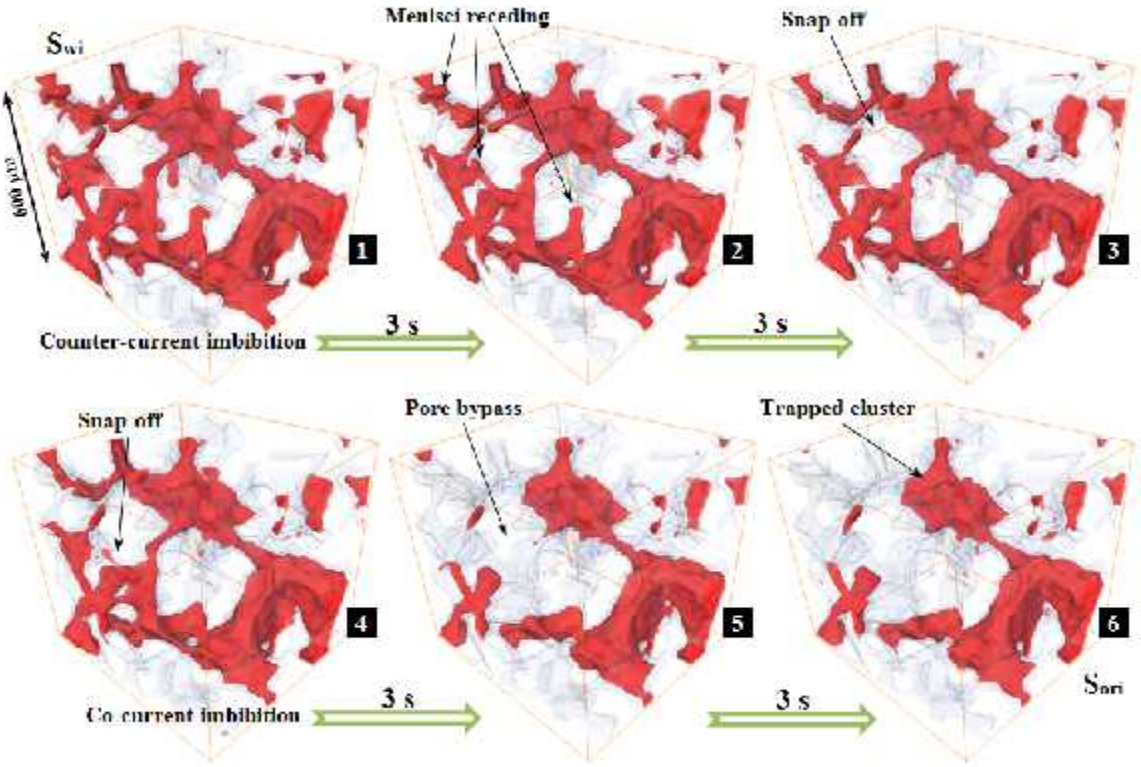

Figure 7 3D images time series of interfaces relaxation and trapping event during spontaneous imbibition with a time interval of 3s and a resolution of 5 µm.

Figure 8 shows a selection of images at different stages of the surfactant injection cycle. These images illustrate at first the complexity of the structure and mechanisms involved at the pore scale. Image 1 and 2 are captured respectively at the beginning and the end of the first stage of surfactant injection. They show that at this low flow rate oil is not mobilized. Nevertheless we can see that during this stage a cluster can break up and coalesce with an adjacent cluster. At the end of the second flow rate (image 3) we see that new connections between clusters have been established and we can note also the presence of small ganglia. During the third stage (image 4 to 6) we can see the evacuation of an oil cluster. First the cluster breaks up by snap-off or pull-off and then it begins to move leaving behind it a number of small ganglia.

To get more insight in the evolution of oil ganglia population, we have extracted some statistical properties from the 3D images of the surfactant injection time-series. In Figure 9 (a) we report the number of cluster as well as the size of the largest cluster as a function of the time. As mentioned previously the surfactant injection rate was increased each 30 s. This graphic shows that at the beginning of the second and the third stage of surfactant injection at respectively 30 s and 60 s, as soon as the injection rate is increased the size of the largest cluster increases immediately as well and then it decreases.

This behavior can be explained as fallow. Once the capillary number has reached a sufficiently high value (critical capillary number) oil clusters menisci begin to move. As the IFT is relatively low menisci can merge as soon as they get in contact leading to clusters coalescence and increasing in this way the size of the largest cluster. Afterwards this largest cluster is partially evacuated from the sample. This is evidenced by Figure 9 (b) where we can see the evolution of the largest cluster in the time interval of 33 s and 42 s. In parallel to that we can see that the number of clusters increases also at the beginning of the second and third stage which corresponds probably to an increase in cluster break up events.

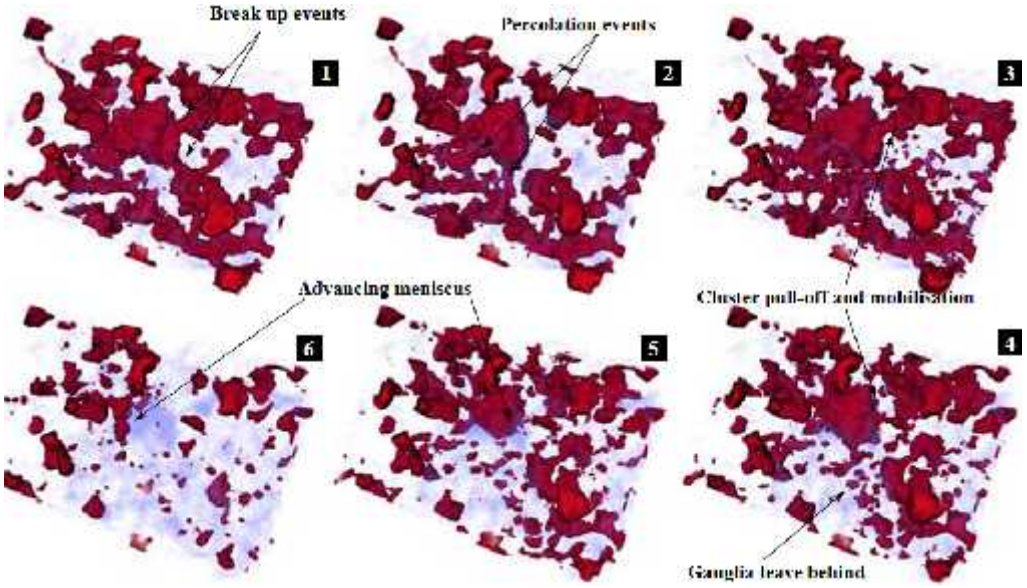

Figure 8 3D images time series during surfactant injection showing different events taking place at the pore scale and resulting in oil cluster mobilization.

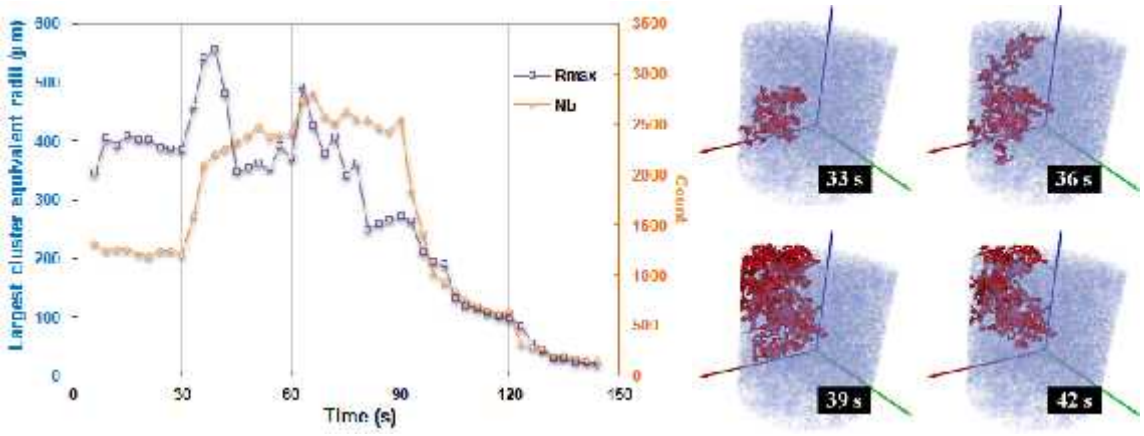

(a) (b)

Figure 9 (a) Evolution of the largest cluster size (R_{max}) and the number of clusters (N_b) as a function of the time. (b) Formation and progression of the largest cluster in the time interval 33s to 42s.

The evolution of the mean cluster size and the relative oil saturation (S_{or}^* defined as the oil saturation divided by the initial residual oil saturation of the surfactant injection cycle) as a function of time are presented in Figure 10 (a). The mean cluster size (R_b) as well as the relative oil saturation decrease at each injection stage as can be expected. In Figure 10 (b) we have reported the mean cluster size at the end of each stage as a function the capillary number expressed as $V_s\ \mu/\sigma$ where V_s and μ are respectively the superficial velocity and viscosity of the surfactant solution and σ the interfacial tension. We found that relation between R_b and the capillary number can be approximated by a power low.

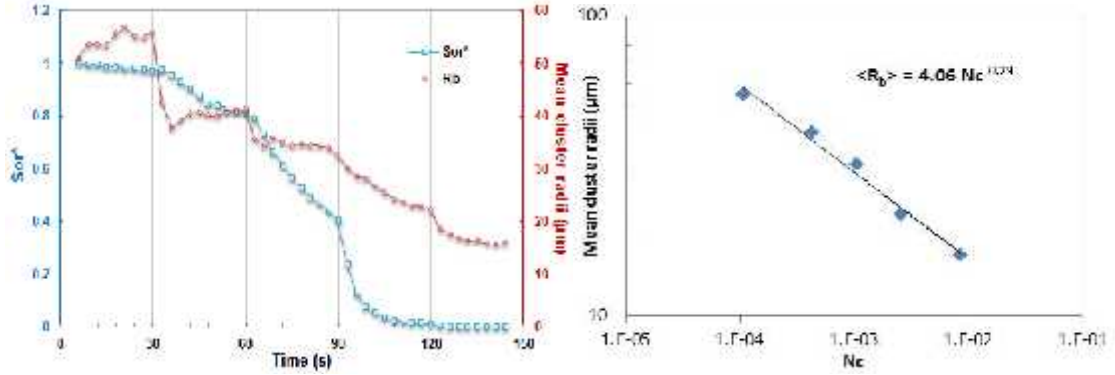

(a) (b)

Figure 10 (a) Evolution of the mean cluster size (R_b) and as the relative oil saturation (S_{or}^*) as a function of the time. (b) mean cluster size versus the capillary number.

CONCLUSION

By combining the ultra-fast microtomography capability developed at the TOMCAT beam line and a dedicated in-situ experimental setup for fluid flow in porous media, we were able to perform and image a drainage, a spontaneous imbibition and a surfactant flooding at different flow rates in a sandstone with a voxel size of 5 µm and a temporal resolution of 3 s. Phase contrast images allowed a good visualization of the fluids flow at the pore scales giving in this way valuable information on the trapping mechanisms and oil ganglion dynamics. We have seen that during surfactant flooding oil clusters coalesce and break up. At intermediate capillary number and high to intermediate residual saturation oil is evacuated by forming large clusters. This behavior is likely to be at the origin of oil bank formation. Finally the mean cluster size was found to be a power law of the capillary number. Further theoretical works will be undertaken to explain this behavior as well as other rock type will be investigated to confirm the observations made during this work.

REFERENCES

1. Chatzis, I., M.S. Kuntamukkula, and N.R. Morrow: "Effect of capillary number on the microstructure of residual oil in strongly water-wet sandstones," *SPE Reservoir Engineering* (1988), 902

2. G.L. Stegemeier: "Mechanisms of entrapment and mobilization of oil in porous media," Academic Press, New York, (1977) 55-91.

3. Lenormand, R., C. Zarcone, and A. Sarr: "Mechanisms of the Displacement of One Fluid by Another in A Network of Capillary Ducts," *Journal of Fluid Mechanics* (1983), 337-353.

4. Chatzis, I. and F.A.L. Dullien: "Dynamic immiscible displacement mechanisms in pore doublet - Theory versus experiment," *Journal of Colloid and Interface Science* (1983), 199-222.

5. Youssef, S., H. Deschamps, J. Dautriat, E. Rosenberg, R. Oughanem, E. Maire, and R. Mokso: "4D imaging of fluid flow dynamics in natural porous media by ultra-fast X-ray microtomography", *Int. Sym. of the Society of Core Analysts*, Napa Valley, California (2013) .

6. Berg, S., H. Ott, S.A. Klapp, A. Schwing, R. Neiteler, N. Brussee, A. Makurat, L. Leu, F. Enzmann, J.O. Schwarz, M. Kersten, S. Irvine, and M. Stampanoni: "Real-time 3D imaging of Haines jumps in porous media flow," *Proceedings of the National Academy of Sciences of the United States of America* (5-3-2013), 3755-3759.

7. Oughanem, R., S. Youssef, Y. Peysson, B. Bazin, E. Maire, and O. Vizika: "Pore-scale to core-scale study of capillary desaturation curves using multi-scale 3D imaging", *Int. Sym. of the Society of Core Analysts*, Napa Valley, California (2013) .

8. Payatakes, A.C., K.M. Ng, and R.W. Flumerfelt: "Oil Ganglion Dynamics During Immiscible Displacement - Model Formulation," *Aiche Journal* (1980), 430-443.

9. Ng, K.M., H.T. Davis, and L.E. Scriven: "Visualization of blob mechanics in flow through porous media," *Chemical Engineering Science* (1978), 1009-1017.

10. Hinkley, R.E., M.M. Dias, and A.C. Payatakes: "On the Motion of Oil Ganglia in Porous-Media," *Physicochemical Hydrodynamics* (1987), 185-211.

11. Avraam, D.G. and A.C. Payatakes: "Flow Regimes and Relative Permeabilities During Steady-State 2-Phase Flow in Porous-Media," *Journal of Fluid Mechanics* (25-6-1995), 207-236.

12. Lenormand, R. and C. Zarcone: "Physics of Blob Displacement in a Two-Dimensional Porous Medium," *SPE Formation Evaluation* (1988), 271-275.

13. Datta, S.S., T.S. Ramakrishnan, and D.A. Weitz: "Mobilization of a trapped non-wetting fluid from a three-dimensional porous medium," *Physics of Fluids* (2014),

14. Berg, S. et all.: "Multiphase flow in porous rock imaged under dynamic flow conditions with fast x-ray computed microtomography", *Int. Sym. of the Society of Core Analysts*, Napa Valley, California (2013)

15. Mokso, R., F. Marone, D. Haberthur, A. Isenegger, G. ikuljan, J.C. Schittny, and M. Stampanoni: "Following Dynamic Processes by X-ray Tomographic Microscopy with Sub-second Temporal Resolution", *International Conference on X-ray Microscopy, AIP Conference Proceedings 1365*, (2011) ,38

16. Youssef, S., D. Bauer, S. Bekri, E. Rosenberg, and O. Vizika: "Towards a better understanding of Multiphase flow in porous media: 3D In-Situ fluid distribution imaging at the pore scale", *Int. Sym. of the Society of Core Analysts*, Noordwijk aan Zee, The Netherlands (2009) .

17. Stampanoni, M., A. Groso, A. Isenegger, G. Mikuljan, Q. Chen, A. Bertrand, S. Henein, R. Betemps, P. Böhler, D. Meister, M. Lange, and R. Abela: "Trends in synchrotron-based tomographic imaging: the SLS experience", *Developments in X-Ray Tomography V, Proc. SPIE 6318,* (2006) .

18. Mokso, R., F. Marone, S. Irvine, M. Nyvlt, D. Schwyn, K. Mader, G.K. Taylor, H.G. Krapp, M. Skeren, and M. Stampanoni: "Advantages of phase retrieval for fast x-ray tomographic microscopy," *Journal of Physics D-Applied Physics* (11-12-2013),

19. Paganin, D., S.C. Mayo, T.E. Gureyev, P.R. Miller, and S.W. Wilkins: "Simultaneous phase and amplitude extraction from a single defocused image of a homogeneous object," *Journal of Microscopy-Oxford* (2002), 33-40.

20. Marone, F. and M. Stampanoni: "Regridding reconstruction algorithm for real-time tomographic imaging," *Journal of Synchrotron Radiation* (2012), 1029-1037.

21. Youssef, S., E. Rosenberg, N. Glan, S. Bekri, and O. Vizika: "Quantitative 3D characterisation of the pore space of real rocks : improved µ-CT resolution and pore extraction methodology", *Int. Sym. of the Society of Core Analysts*, Calgary, Canada (2007)